CDF Note 10636

Search for trilepton new physics and chargino-neutralino production at the Collider Detector at Fermilab

The CDF Collaboration
(http://www-cdf.fnal.gov)

February 17, 2013

Abstract

We perform a search for new physics in general and chargino-neutralino in particular, in the trilepton $+\not\!\!E_T$ channels, using 5.8 fb^{-1} of CDF Run II data. We investigate ee+lepton and $\mu\mu$+lepton final states, where lepton can be an electron, a muon, a hadronic tau, or an isolated track. Compared to the previous trilepton CDF analysis, we expand our acceptance to the forward region of the detector, we include a hadronically-decaying tau as a third lepton, and we use the lowest momenta for our leptonic objects (some times down to 5 GeV/c) within the constraints of the object identification and trigger requirements. We study the event yields and kinematics in 24 dilepton and 40 trilepton standard-model dominated control regions, defined in the dilepton-mass vs $\not\!\!E_T$ vs jet-multiplicity phase space. After observing good agreement between data and SM expectation in the control regions, we investigated the signal region at the end of the analysis. Although some excess is seen, the results are consistent with the SM predictions. These results are used for setting limits on the chargino-neutralino production, where we exclude cross-sections > 0.1 fb and chargino masses < 168 GeV/c^2 at 95% CL, for the mSUGRA parameters $m_0 = 60$ GeV/c^2, $\tan\beta = 3$, and $A_0 = 0$. A region in the $m_{1/2}$ vs. m_0 mSUGRA parameter space is also excluded at 95% CL.

I. INTRODUCTION

The main motivation for the trilepton analysis is a potential $\tilde{\chi}_1^{\pm}\tilde{\chi}_2^0$ chargino-neutralino supersymmetry (SUSY) signal at the Tevatron. Here $\tilde{\chi}_1^{\pm}$ is the lightest of the two charginos predicted and $\tilde{\chi}_2^0$ is the next-to-lightest of the four neutralinos. Eventually both particles will decay to SM particles and the lightest neutralino, which is the lightest supersymmetric particle (LSP) in the mSUGRA scenario. Under R-parity conservation, the LSP neutralino will be stable and will not interact with the detector, which will lead to missing transverse energy ($\not\!\!E_T$). This is the most promising SUSY signal at the collider, given the existing limits on the mass of the gluino (> 300 GeV/c^2 at 95% CL [1, 2]), which reduces considerably the available kinematic space for the production of squarks and gluinos. In addition, the trilepton mode of the gaugino decays is characterized by very low standard model (SM) backgrounds. For these reasons, the trilepton final state is considered to be the golden Tevatron SUSY signature.

Previously, CDF performed trilepton searches with 1 fb^{-1} [3–5], 2 fb^{-1} [6], and 3.2 fb^{-1} [7] of Run II data. The latest DØ trilepton analysis [8] used 2.3 fb^{-1} of data. We present here a 5.8 fb^{-1} analysis. Compared to the previous trilepton CDF analysis, we expand our acceptance to the forward region of the detector, we include third taus decaying hadronically and we use the lowest momenta for our leptonic objects (some times down to 5 GeV/c) within the constraints of the object identification and trigger requirements. The inclusion of tau leptons is also motivated by the high branching ratio of supersymmetric decays to the lightest slepton, which is usually the stau, and which always decays to a tau lepton.

II. THE CDF II DETECTOR

CDF II [9] is a multi-purpose cylindrical detector with projective-tower calorimeter geometry and excellent lepton identification capability. It operates at Fermilab's Tevatron collider where protons and antiprotons collide with a center-of-mass energy of 1.96 TeV. In CDF's coordinate system the positive $\vec{z}$-axis is defined by the proton beam direction and the positive $\vec{y}$-axis by the vertical upward direction. The detector is approximately symmetric in the η and ϕ directions, where the pseudorapidity η is defined as $\eta = -\ln[\tan(\theta/2)]$, θ is the polar angle with respect to $\vec{z}$, and ϕ is the azimuthal angle.

The momentum p of charged particles is measured with a tracking system composed of an eight-layer silicon strip detector and a 96-layer drift chamber; both are located inside

a solenoid providing a magnetic field of 1.4 T aligned along the beam axis. The tracking efficiency is nearly 100% in the central region ($|\eta| < 1$) and decreases in the forward region ($1 < |\eta| < 2.8$). Electromagnetic and hadronic calorimeters surround the solenoid and measure the energies of collision products up to $|\eta| = 3.6$. Drift chambers and scintillators are installed around the hadronic calorimeter to detect muons with $|\eta| < 1.4$. Gas Cherenkov counters measure the average number of inelastic $p\bar{p}$ collisions per bunch crossing and thereby determine the beam luminosity. A pipelined three-level trigger system [10] that combines hardware and software is used for filtering the collision data.

III. EVENT SELECTION

We use data collected with high-p_T ($p_T > 18$ GeV/c) central single-electron and single-muon triggers and corresponding to 5.8 fb^{-1} of integrated luminosity. To ensure constant trigger response, we require at least one central electron or muon with $p_T > 20$ GeV/c. The second and the third lepton should have any momentum above 5 GeV/c. We start with two leptons of the same flavor (electron or muon) and we look for a third one that can be an electron, muon, tau (decaying hadronically) or an isolated track. Tau leptons that decay leptonically will become apparent to us through their soft lepton decay products. All leptons should be isolated (calorimeter-based absolute or relative isolation (depending on their p_T) for e, μ, τ leptons, track-based isolation for the third isolated track). Special care is taken to reduce decays-in-flight contamination that affect the track-based momentum determination of muons in the dimuon high-mass spectrum. Jets are reconstructed with an algorithm (JETCLU [11]) based on a cone of size $\Delta R = \sqrt{(\Delta\phi)^2 + (\Delta\eta)^2} = 0.4$ and they are counted if they are not consistent with electrons (in location or in fraction of their energy deposited in the electromagnetic calorimeter), and if they have transverse energy above 20 GeV and pseudorapidity less than 2.5. They also have to be $\Delta R > 0.4$ away from any leptonic object. The missing transverse energy $\not\!\!E_T$ is corrected for the electron and jet calibrations and for the presence of muons and isolated tracks that minimally interact with the calorimeter. To reduce fake $\not\!\!E_T$, we reject events from the high-$\not\!\!E_T$ control and signal regions, if they have leptons with $\Delta\phi(\text{lep}, \not\!\!E_T) < 20^\circ$ or jets (of transverse energy $E_T > 10$ GeV) with $\Delta\phi(\text{jet}, \not\!\!E_T) < 20^\circ$. All events are required to have a high-quality primary vertex close to the leptons, and to pass the photon-conversion-removal and cosmic-ray reduction cuts.

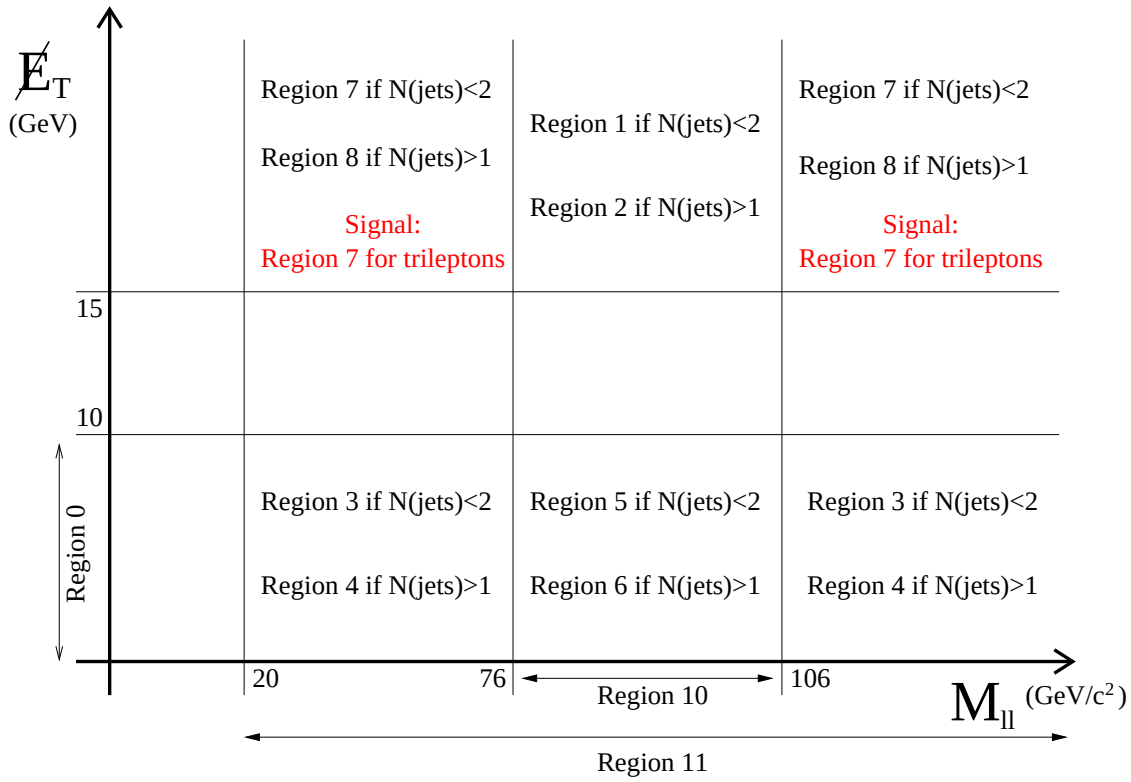

FIG. 1: Dilepton and trilepton control regions used for the validation of our SM backgrounds. Region 7 for trileptons is the signal region.

IV. STANDARD MODEL BACKGROUNDS

Understanding of the SM backgrounds is the single most important goal in the search of new physics. For this reason, we define 24 dilepton and 40 trilepton control regions where we do not expect chargino-neutralino signal and where we validate our background estimations. The control regions are defined in the kinematic space defined by variation of three variables: the dilepton invariant mass $M_{\ell\ell}$, the transverse missing energy $\not\!\!E_T$, and the jet multiplicity $N_{\rm jet}$. Figure 1 and Table I define our control regions. We have 12 ee and 12 $\mu\mu$ control regions. For trileptons, we exclude regions 7 and 9 (signal and signal-like regions, which we investigate at the end), so we have 10 control regions per ee+lepton, ee+track, $\mu\mu$+lepton, $\mu\mu$+track for a total of 40 trilepton control regions. Since we do not fit any part of our background to the data, there is a chance for discovery of new phenomena in the control regions as well.

Definition of Control and Signal Regions			
Region	$M_{\ell\ell}$ **cut (Gev/c^2)**	($\not\!\!E_T$) **cut (GeV)**	N_{jet} **cut**
Region0	$M_{\ell\ell} > 20$	$\not\!\!E_T < 10$	–
Region1	$76 < M_{\ell\ell} < 106$	$\not\!\!E_T > 15$	$N_{jet} \leq 1$
Region2	$76 < M_{\ell\ell} < 106$	$\not\!\!E_T > 15$	$N_{jet} \geq 2$
Region3	$20 < M_{\ell\ell} < 76$ or $M_{\ell\ell} > 106$	$\not\!\!E_T < 10$	$N_{jet} \leq 1$
Region4	$20 < M_{\ell\ell} < 76$ or $M_{\ell\ell} > 106$	$\not\!\!E_T < 10$	$N_{jet} \geq 2$
Region5	$76 < M_{\ell\ell} < 106$	$\not\!\!E_T < 10$	$N_{jet} \leq 1$
Region6	$76 < M_{\ell\ell} < 106$	$\not\!\!E_T < 10$	$N_{jet} \geq 2$
Region7	$20 < M_{\ell\ell} < 76$ or $M_{\ell\ell} > 106$	$\not\!\!E_T > 15$	$N_{jet} \leq 1$
Region8	$20 < M_{\ell\ell} < 76$ or $M_{\ell\ell} > 106$	$\not\!\!E_T > 15$	$N_{jet} \geq 2$
Region9	$20 < M_{\ell\ell} < 76$ or $M_{\ell\ell} > 106$	$\not\!\!E_T > 20$	$N_{jet} \leq 1$
Region10	$76 < M_{\ell\ell} < 106$	–	–
Region11	$M_{\ell\ell} > 20$	–	–

TABLE I: The signal and control regions used in our analysis, for both dilepton and trileptons. Region 7 for trileptons is the signal region.

A. Dilepton backgrounds

The main SM background to the dilepton final states comes from the Drell-Yan (DY) process $p\bar{p} \to Z^*/\gamma \to \ell\ell$, which is estimated using PYTHIA [12] Monte Carlo (MC) simulated events generated with the CTEQ5L [13] parton distribution functions, processed by the GEANT-based [14] CDF detector simulator. The MC is normalized using next-to-leading order (NLO) theoretical cross sections [15], lepton-ID scale factors, trigger efficiencies, and the data luminosity. Validation of the DY confirms this normalization. At lower dilepton invariant masses $M_{\ell\ell}$ fake-lepton background is present. This background consists mainly of one real lepton and a hadronic jet or isolated track that fakes a second lepton. Usual source of this background is the W+jets events. The background is estimated in two steps [16]. First the probability that a generic hadronically-originated jet (track) fakes an electron or tau (muon, leptonic isolated track) is determined with CDF jet-rich data. Then this probability is applied to all fakeable jets and tracks in events with one identified lepton. Figure 2 shows the inclusive dielectron and dimuon mass spectrum (Region 11), where the contributions from the DY and fake backgrounds are evident and our estimation of these backgrounds is validated. Understanding of the $\not\!\!E_T$ distribution is very important in high-$\not\!\!E_T$ searches. Figures 3 shows the inclusive dielectron and dimuon $\not\!\!E_T$ distribution (Region 11), where we observe good understanding of the backgrounds. The clean-up $\Delta\phi(\text{lep}, \not\!\!E_T)$ and $\Delta\phi(\text{jet}, \not\!\!E_T)$ cuts have not been applied in this control region.

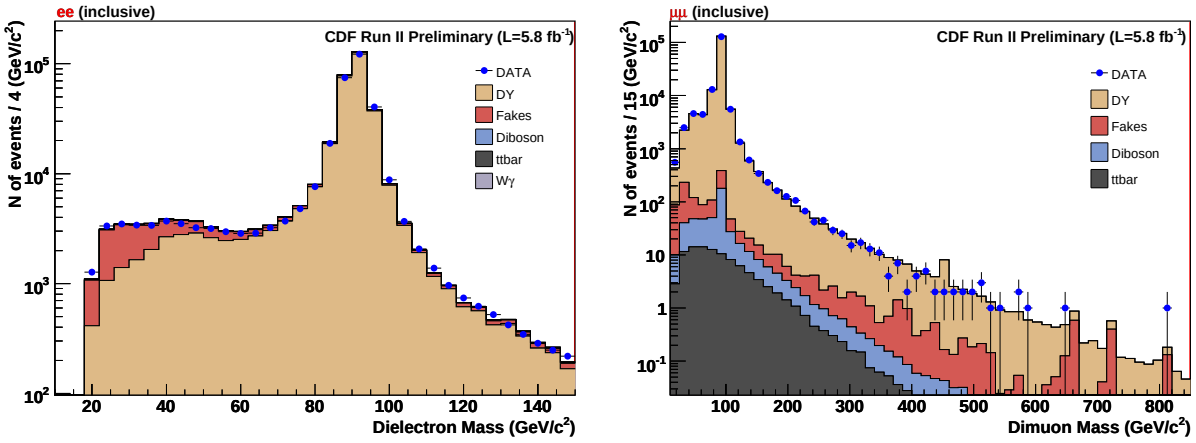

FIG. 2: Dielectron and dimuon mass spectra in the inclusive case.

Minor backgrounds come from diboson events (WW, WZ, ZZ, and $W\gamma$, the latter for dielectron events), which are estimated with the same MC process we use for DY. This background is more evident at the higher $\not\!\!E_T$ ($\not\!\!E_T > 60$ GeV), shown in Figure 3 for dielectrons and dimuons. Finally, the $t\bar{t}$ production with subsequent decays to dileptons is considered. This background contributes non-trivially in the control region with very high $\not\!\!E_T$ ($\not\!\!E_T > 100$ GeV), as shown in Figure 3.

Important dilepton control regions are the ones characterized by $\not\!\!E_T > 15$ GeV, exclusion of the Z-boson and $N_{jet} \leq 1$ (Region 7). These regions have the same kinematic requirements as our signal region, but they require two instead of three leptons. Figures 4 and 5 show the dielectron and dimuon mass spectra, along with the systematic uncertainties, in this region. Good agreement is observed.

Tables II and III show the dielectron and dimuon yields for all control regions. Figure 6 shows the $N_{\rm observed}/N_{\rm expected}$ ratio with an error bar defined as $N_{\rm observed}\delta N_{\rm expected}/N^2_{\rm expected}$, where $N_{\rm observed}$ is the detected number of events per region, $N_{\rm expected}$ is the number of events predicted by the SM, and $\delta N_{\rm expected} = \sqrt{N_{\rm expected} + (\delta N^{\rm syst}_{\rm expected})^2}$ is the total uncertainty on the prediction (including the statistical one), where $\delta N^{\rm syst}_{\rm expected}$ is the systematic uncertainty on the SM prediction.

B. Trilepton backgrounds

The dominant SM background to the trilepton final states comes from fake events, which are events with two identified leptons and a jet (track) faking an electron or tau (muon, isolated track). The main origin of this background is DY+jets and it is estimated with

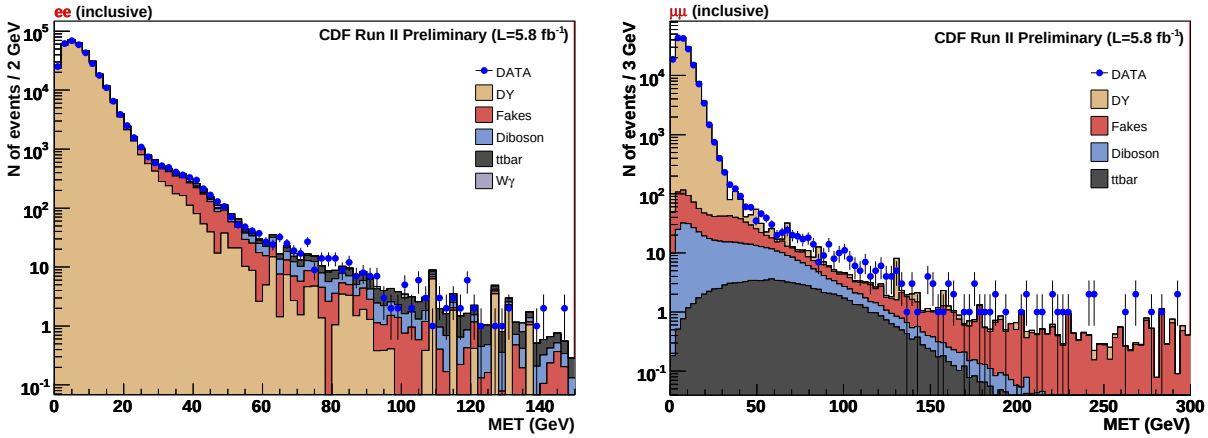

FIG. 3: Dielectron and dimuon $\not\!\!E_T$ spectra in the inclusive case.

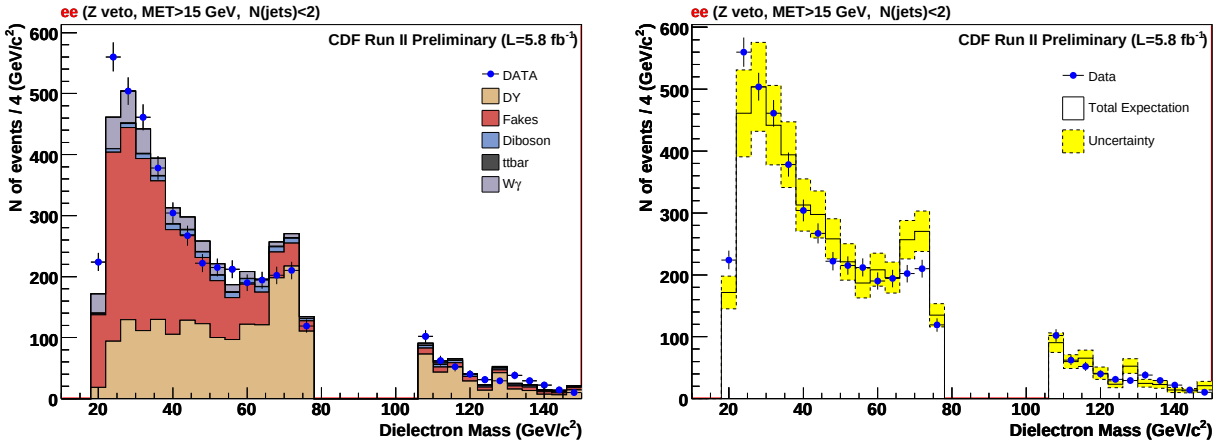

FIG. 4: Dielectron spectrum for events with $\not\!\!E_T > 15$ GeV, $N_{\rm jet} \leq 1$ and exclusion of Z resonance. Right-hand plot shows the SM prediction systematic uncertainty.

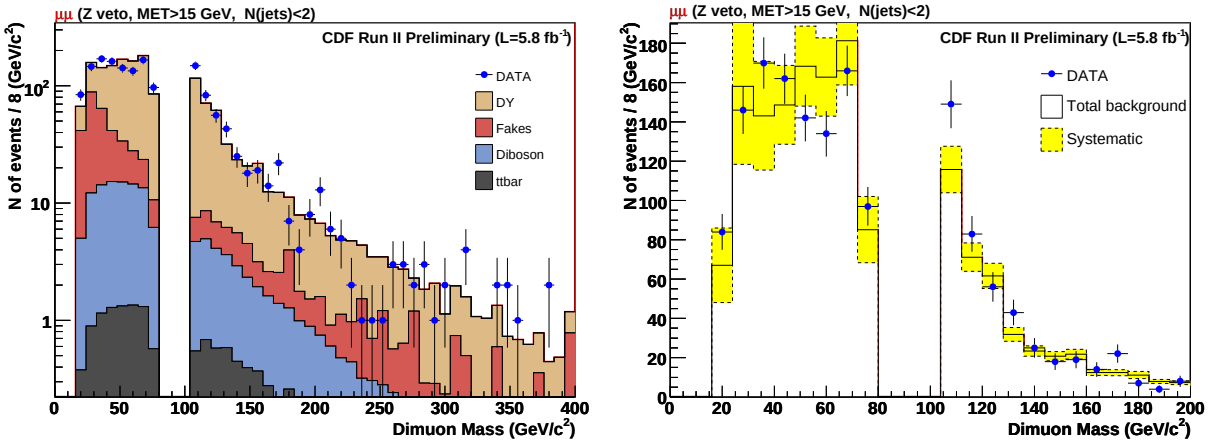

FIG. 5: Dimuon spectrum for events with $\not\!\!E_T > 15$ GeV, $N_{\rm jet} \leq 1$ and exclusion of Z resonance. Right-hand plot shows the SM prediction systematic uncertainty.

Table of dielectron yields (CDF Run II Preliminary, L=5.8 fb^{-1})							
	Drell-Yan	Fakes	Diboson	$W+\gamma$	Top	Total SM	Observed
Region0	251266 ± 25133	12261 ± 4234	124 ± 12	12 ± 2	2.6 ± 0.3	263666 ± 25500	**257588**
Region1	9942 ± 1004	387 ± 172	103 ± 10	35 ± 5	5.2 ± 0.5	10472 ± 1033	**10077**
Region2	359 ± 43	22 ± 9	11 ± 1	0.7 ± 0.5	16 ± 2	407 ± 46	**506**
Region3	29663 ± 2969	7711 ± 2139	16 ± 2	11 ± 2	0.49 ± 0.06	37401 ± 3661	**36538**
Region4	396 ± 45	285 ± 80	5.5 ± 0.5	0 ± 0	1.5 ± 0.2	688 ± 92	**727**
Region5	218481 ± 21856	4191 ± 1985	49 ± 5	0.9 ± 0.5	0.13 ± 0.02	222722 ± 21950	**217846**
Region6	2726 ± 280	74 ± 30	54 ± 5	0 ± 0	0.45 ± 0.05	2855 ± 287	**2477**
Region7	2203 ± 226	2152 ± 524	165 ± 16	360 ± 37	19 ± 2	4898 ± 594	**4909**
Region8	66 ± 11	136 ± 38	4.9 ± 0.5	3.2 ± 0.9	56 ± 6	265 ± 42	**338**
Region9	764 ± 83	1620 ± 382	157 ± 16	339 ± 35	72 ± 7	2952 ± 406	**3270**
Region10	263448 ± 26353	4891 ± 2309	282 ± 28	20 ± 3	28 ± 3	268670 ± 26486	**260010**
Region11	324059 ± 32412	20218 ± 6638	527 ± 53	472 ± 48	134 ± 13	345410 ± 33196	**334968**

TABLE II: Dielectron events in all the control regions.

Table of dimuon yields (CDF Run II Preliminary, L=5.8 fb^{-1})						
	Drell-Yan	Fakes	Diboson	Top	Total SM	Observed
Region0	114498 ± 11454	226 ± 113	75 ± 8	1.8 ± 0.2	114802 ± 11455	**115884**
Region1	7926 ± 802	38 ± 19	72 ± 7	3.6 ± 0.4	8039 ± 802	**7272**
Region2	319 ± 40	1.6 ± 0.8	8.8 ± 0.9	12 ± 1	341 ± 40	**308**
Region3	12171 ± 1218	70 ± 35	9.7 ± 1	0.33 ± 0.04	12251 ± 1218	**12729**
Region4	170 ± 18	2 ± 1	3.4 ± 0.3	1.1 ± 0.1	177 ± 18	**199**
Region5	100913 ± 10100	152 ± 76	30 ± 3	0.08 ± 0.01	101095 ± 10100	**101740**
Region6	1244 ± 132	3 ± 1	32 ± 3	0.31 ± 0.04	1279 ± 132	**1216**
Region7	1170 ± 118	273 ± 136	118 ± 12	14 ± 1	1575 ± 181	**1610**
Region8	36 ± 4	9 ± 5	3.7 ± 0.4	41 ± 4	89 ± 7	**125**
Region9	366 ± 37	258 ± 129	113 ± 11	53 ± 5	790 ± 135	**808**
Region10	145635 ± 14572	245 ± 123	202 ± 20	21 ± 2	146103 ± 14573	**142386**
Region11	163932 ± 16397	728 ± 364	364 ± 36	98 ± 10	165122 ± 16401	**162127**

TABLE III: Dimuon events in the control regions.

real CDF data, by applying the fake probability described in the previous section to events with two identified electrons or muons. The main electroweak SM trilepton background comes from DY+γ, where the photon converts to an electron and positron which almost always are reconstructed as a single electron. Figure 7 shows the inclusive dielectron and dimuon mass spectrum of trilepton events, where the contributions from the DY+γ and fake backgrounds are evident and our estimation of these backgrounds is validated. Figure 8 shows the corresponding $\not\!\!E_T$ distributions.

Minor trilepton backgrounds comes from diboson, more evidently at the high-$\not\!\!E_T$ ($\not\!\!E_T >$

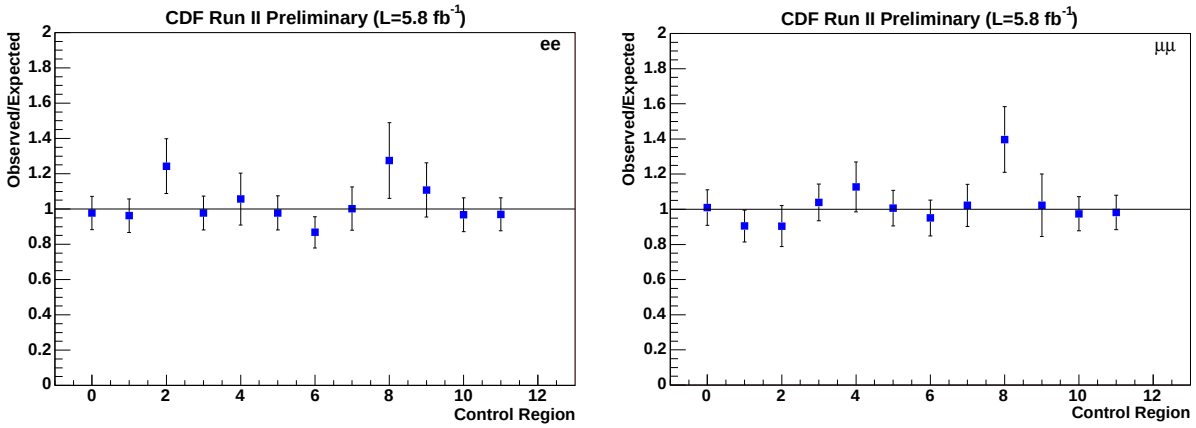

FIG. 6: Dielectron and dimuon $N_{\rm observed}/N_{\rm expected}$ ratio for the control regions.

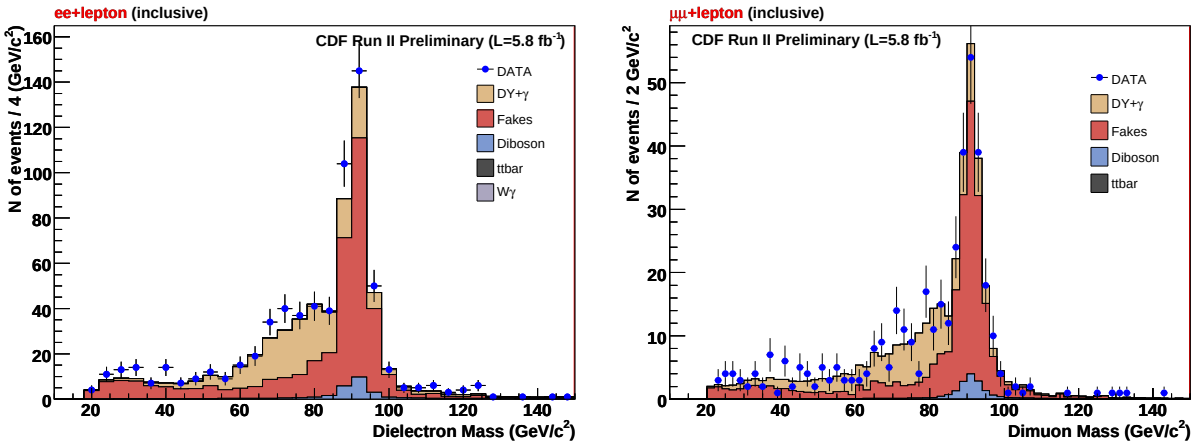

FIG. 7: Dielectron and dimuon mass spectra for ee+lepton and $\mu\mu$+lepton events in the inclusive case.

40 GeV), low jet multiplicity, Z-boson region (Region 1), shown in Figures 9 and 10 for ee+lepton and $\mu\mu$+lepton and for the mass spectrum and $\not\!\!E_T$ distributions. These plots confirm our understanding of the diboson background. The $t\bar{t}$ production is also considered, although it trivially affects only the high-$\not\!\!E_T$ and high-jet-multiplicity regions.

In the trilepton control regions we study separately the ee+track and the $\mu\mu$+track events, because they are dominated exclusively by the fake background. Figures 11 and 12 show the mass spectrum and $\not\!\!E_T$ distribution for those events.

Tables IV-VII list the ee+lepton, ee+track, the $\mu\mu$+lepton, and $\mu\mu$+track yields for all control regions. Figures 13 and 14 show the $N_{\rm observed}/N_{\rm expected}$ ratio for these regions. For the two control regions with $N_{\rm observed} = 0$ ($\mu\mu$+lepton control regions 4 and 8), the error shown is $\delta N_{\rm expected}/N^2_{\rm expected}$.

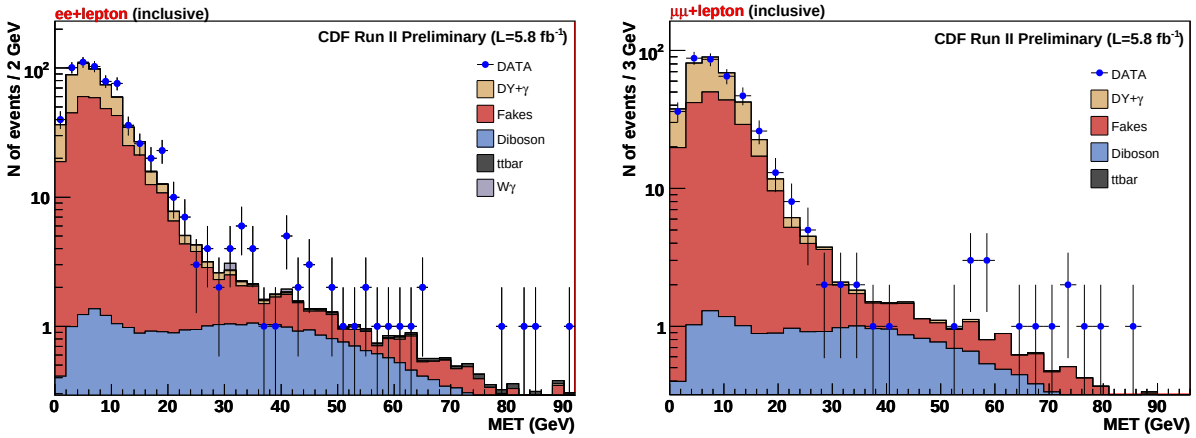

FIG. 8: Distribution of $\not\!\!E_T$ for ee+lepton and $\mu\mu$+lepton events in the inclusive case.

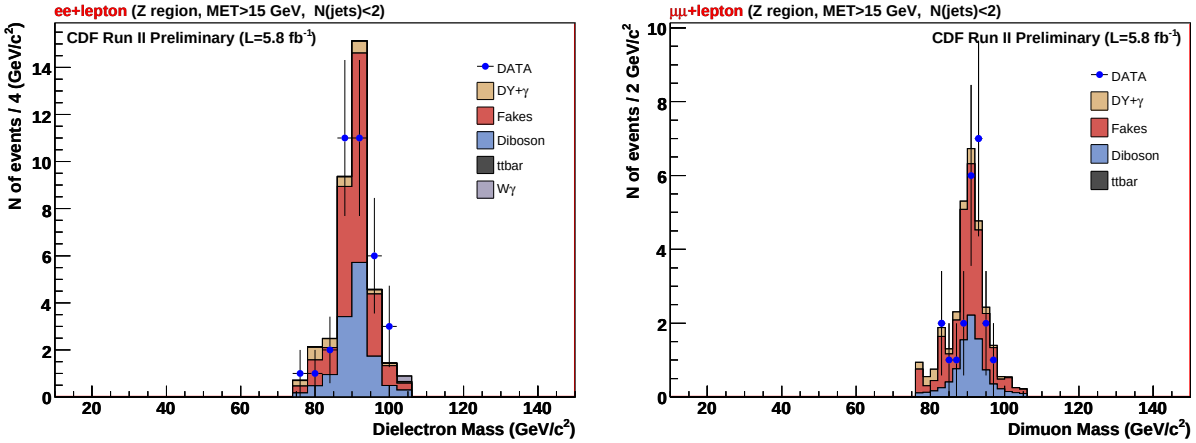

FIG. 9: Dielectron and dimuon mass spectra for ee+lepton and $\mu\mu$+lepton events with $M_{\ell\ell}$ in the Z-boson resonance and with $\not\!\!E_T > 15$ GeV, $N_{\rm jet} \leq 1$.

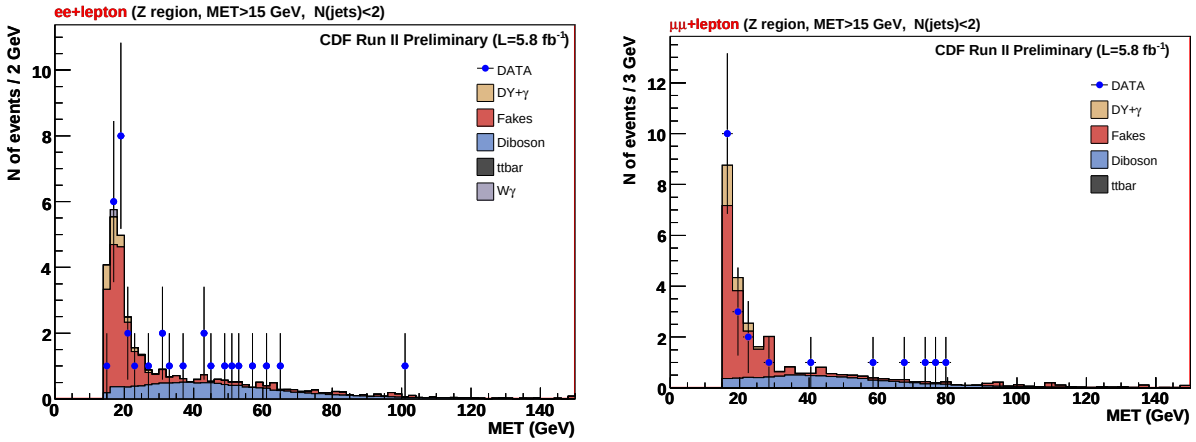

FIG. 10: Distribution of $\not\!\!E_T$ for ee+lepton and $\mu\mu$+lepton events with $M_{\ell\ell}$ in the Z-boson resonance and with $\not\!\!E_T > 15$ GeV, $N_{\rm jet} \leq 1$.

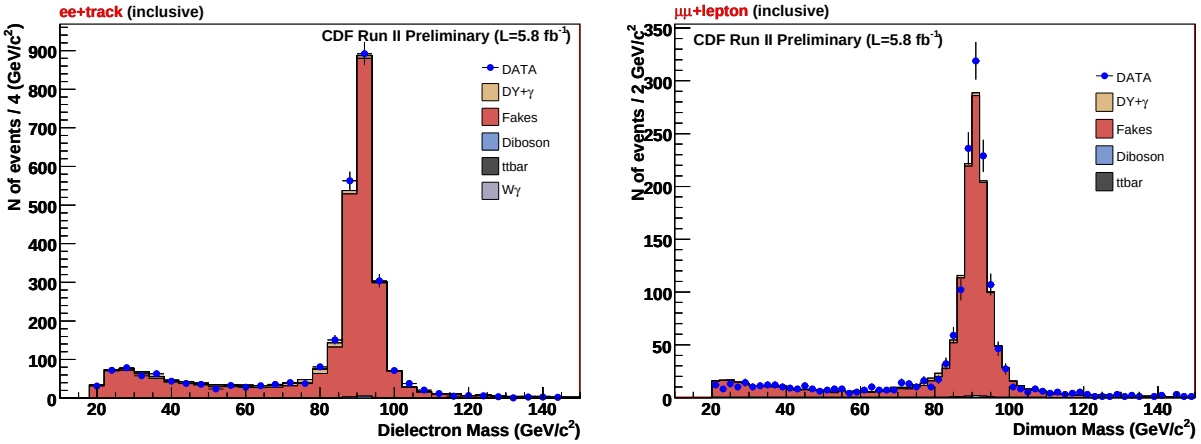

FIG. 11: Distribution of $\not\!\!E_T$ for ee+track and $\mu\mu$+track events in the inclusive case.

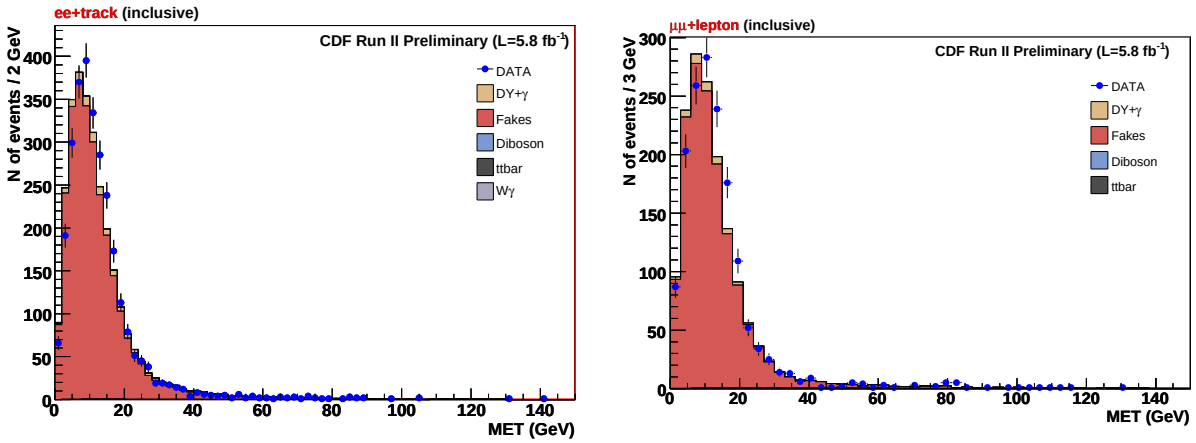

FIG. 12: Distribution of $\not\!\!E_T$ for ee+track and $\mu\mu$+track events in the inclusive case.

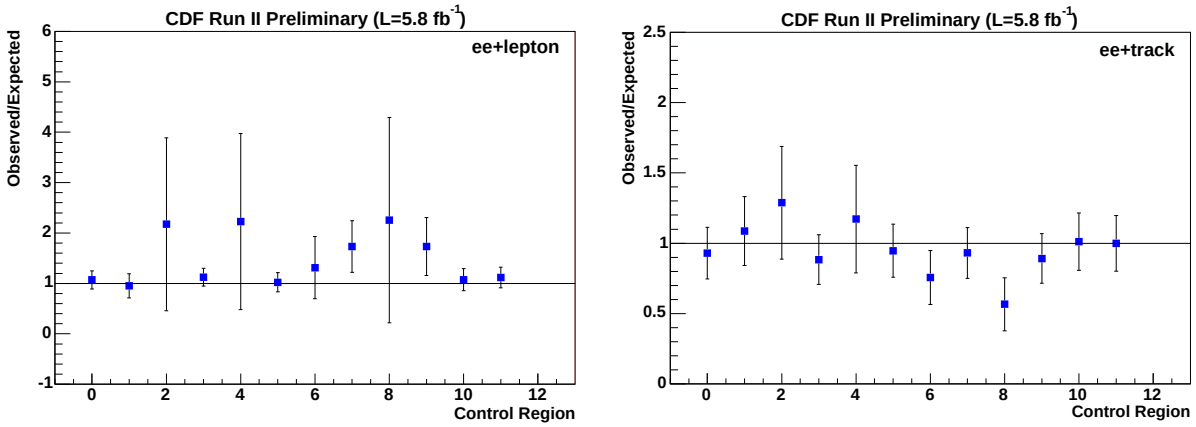

FIG. 13: $N_{\text{observed}}/N_{\text{expected}}$ ratio for ee+lepton (left) and ee+track (right) for all control and signal regions.

Table of ee+lepton yields (CDF Run II Preliminary, L=5.8 fb^{-1})							
	Drell-Yan	Fakes	Diboson	$W+\gamma$	Top	Total SM	Observed
Region0	174 ± 17	226 ± 63	5.2 ± 0.5	0 ± 0	0.041 ± 0.009	406 ± 65	**434**
Region1	2.4 ± 0.3	21 ± 7	13 ± 1	0.2 ± 0.2	0.13 ± 0.02	37 ± 7	**35**
Region2	0.13 ± 0.03	1.4 ± 0.5	0.26 ± 0.03	0 ± 0	0.06 ± 0.01	1.8 ± 0.5	**4**
Region3	86 ± 9	59 ± 18	1.9 ± 0.2	0 ± 0	0.026 ± 0.007	147 ± 20	**165**
Region4	0.51 ± 0.07	1.2 ± 0.4	0.075 ± 0.009	0 ± 0	0.008 ± 0.004	1.8 ± 0.4	**4**
Region5	87 ± 9	161 ± 43	3.1 ± 0.3	0 ± 0	0.002 ± 0.002	251 ± 44	**257**
Region6	0.77 ± 0.1	5 ± 1	0.15 ± 0.02	0 ± 0	0.005 ± 0.003	6 ± 1	**8**
Region7	3.1 ± 0.3	10 ± 4	5.9 ± 0.6	0.1 ± 0.1	0.44 ± 0.05	20 ± 4	**34**
Region8	0.09 ± 0.02	0.9 ± 0.3	0.12 ± 0.01	0 ± 0	0.25 ± 0.03	1.3 ± 0.3	**3**
Region9	0.9 ± 0.1	7 ± 3	5.5 ± 0.6	0.1 ± 0.1	0.66 ± 0.07	14 ± 3	**24**
Region10	94 ± 9	243 ± 69	20 ± 2	0.2 ± 0.2	0.21 ± 0.03	358 ± 70	**385**
Region11	215 ± 22	371 ± 108	34 ± 3	0.7 ± 0.4	1.3 ± 0.1	621 ± 111	**687**

TABLE IV: ee+lepton event yields in the control and the signal regions.

Table of ee+track yields (CDF Run II Preliminary, L=5.8 fb^{-1})							
	Drell-Yan	Fakes	Diboson	$W+\gamma$	Top	Total SM	Observed
Region0	39 ± 4	1380 ± 277	1.7 ± 0.2	0 ± 0	0.019 ± 0.006	1420 ± 277	**1321**
Region1	6.6 ± 0.7	249 ± 57	5.8 ± 0.6	0.4 ± 0.2	0.08 ± 0.01	262 ± 57	**285**
Region2	0.25 ± 0.04	18 ± 4	0.59 ± 0.06	0 ± 0	0.2 ± 0.03	19 ± 4	**25**
Region3	15 ± 2	290 ± 58	0.27 ± 0.03	0 ± 0	0.004 ± 0.003	306 ± 58	**270**
Region4	0.28 ± 0.05	15 ± 3	0.065 ± 0.008	0 ± 0	0.013 ± 0.005	15 ± 3	**18**
Region5	23 ± 2	1035 ± 208	0.77 ± 0.08	0 ± 0	0.002 ± 0.002	1058 ± 208	**1002**
Region6	0.35 ± 0.06	40 ± 8	0.59 ± 0.06	0 ± 0	0 ± 0	41 ± 8	**31**
Region7	26 ± 3	124 ± 27	4 ± 0.4	2.4 ± 0.7	0.27 ± 0.04	157 ± 28	**146**
Region8	0.62 ± 0.08	13 ± 3	0.24 ± 0.03	0 ± 0	0.65 ± 0.07	14 ± 3	**8**
Region9	21 ± 2	83 ± 19	4 ± 0.4	2.4 ± 0.7	0.91 ± 0.1	111 ± 19	**99**
Region10	42 ± 4	1890 ± 390	11 ± 1	0 ± 0	0.36 ± 0.04	1942 ± 390	**1964**
Region11	114 ± 11	2707 ± 560	18 ± 2	4 ± 0.9	1.9 ± 0.2	2845 ± 560	**2843**

TABLE V: ee+track event yields in the control and the signal regions.

V. SYSTEMATIC UNCERTAINTIES

The main sources of systematic uncertainty on the MC-estimated backgrounds [17] are the theoretical cross sections (an 8% effect on the event yields), the luminosity (6%), the lepton-ID efficiency (2%), the parton distribution functions (2%), and the trigger efficiency (0.5%). The total MC systematic uncertainty on the expected event yield is $\sim$ 10 %. The respective QCD-background systematic uncertainty is $\sim$ 50 % for fakeable tracks/jets with transverse momentum $>$ 20 GeV/c and $\sim$ 20% for lower transverse momenta. The determination of this systematic uncertainty comes from variations in the measurement of

Table of $\mu\mu$+lepton yields (CDF Run II Preliminary, L=5.8 fb^{-1})						
	Drell-Yan	Fakes	Diboson	Top	Total SM	Observed
Region0	106 ± 11	126 ± 35	3.1 ± 0.3	0.019 ± 0.007	236 ± 37	**234**
Region1	2.6 ± 0.3	19 ± 6	8.7 ± 0.9	0.041 ± 0.01	30 ± 6	**22**
Region2	0.07 ± 0.02	1 ± 0.4	0.17 ± 0.02	0.033 ± 0.009	1.3 ± 0.4	**3**
Region3	53 ± 5	26 ± 8	0.64 ± 0.07	0.015 ± 0.006	80 ± 9	**85**
Region4	0.34 ± 0.06	0.5 ± 0.2	0.025 ± 0.004	0.004 ± 0.003	0.8 ± 0.2	**0**
Region5	52 ± 5	98 ± 26	2.4 ± 0.2	0 ± 0	152 ± 27	**145**
Region6	0.5 ± 0.08	2.3 ± 0.7	0.1 ± 0.01	0 ± 0	3 ± 0.7	**4**
Region7	2.6 ± 0.3	7 ± 2	3.3 ± 0.3	0.23 ± 0.03	13 ± 2	**19**
Region8	0.09 ± 0.03	0.4 ± 0.1	0.08 ± 0.01	0.13 ± 0.02	0.7 ± 0.1	**0**
Region9	0.64 ± 0.1	4 ± 1	3.1 ± 0.3	0.35 ± 0.04	9 ± 1	**6**
Region10	72 ± 7	170 ± 49	15 ± 2	0.09 ± 0.02	257 ± 49	**250**
Region11	144 ± 14	224 ± 65	21 ± 2	0.63 ± 0.07	391 ± 67	**398**

TABLE VI: $\mu\mu$+lepton event yields in the control and the signal regions.

Table of $\mu\mu$+track yields (CDF Run II Preliminary, L=5.8 fb^{-1})						
	Drell-Yan	Fakes	Diboson	Top	Total SM	Observed
Region0	19 ± 2	695 ± 140	1 ± 0.1	0.017 ± 0.006	714 ± 140	**641**
Region1	3.3 ± 0.4	169 ± 38	3.5 ± 0.4	0.033 ± 0.009	176 ± 38	**183**
Region2	0.06 ± 0.02	12 ± 3	0.4 ± 0.04	0.14 ± 0.02	12 ± 3	**16**
Region3	6.6 ± 0.7	128 ± 26	0.13 ± 0.02	0.004 ± 0.003	135 ± 26	**116**
Region4	0.14 ± 0.04	5 ± 1	0.037 ± 0.006	0.011 ± 0.005	5 ± 1	**8**
Region5	12 ± 1	540 ± 109	0.48 ± 0.05	0 ± 0	552 ± 109	**498**
Region6	0.29 ± 0.06	21 ± 4	0.36 ± 0.04	0.002 ± 0.002	22 ± 4	**19**
Region7	2.8 ± 0.3	65 ± 15	2.3 ± 0.2	0.18 ± 0.03	70 ± 15	**62**
Region8	0.1 ± 0.03	5 ± 1	0.12 ± 0.01	0.47 ± 0.06	5 ± 1	**2**
Region9	1.5 ± 0.2	45 ± 10	2.3 ± 0.2	0.64 ± 0.07	49 ± 10	**38**
Region10	25 ± 3	1151 ± 238	7.3 ± 0.7	0.24 ± 0.03	1184 ± 238	**1221**
Region11	43 ± 4	1463 ± 303	12 ± 1	1.2 ± 0.1	1518 ± 303	**1560**

TABLE VII: $\mu\mu$+track event yields in the control and the signal regions.

the fake probabilities using different jet-rich CDF datasets triggered with varied jet-energy thresholds. The jet-energy systematic uncertainty affects both the jet counting, and the missing transverse energy (which is corrected for the jet energy). As a result, the effect of this systematic uncertainty migrates events across the control/signal regions and also affects the $\not\!\!E_T$ distribution. We measured the effect of this uncertainty to be $< 0.2\%$ in the signal region, so we ignore it.

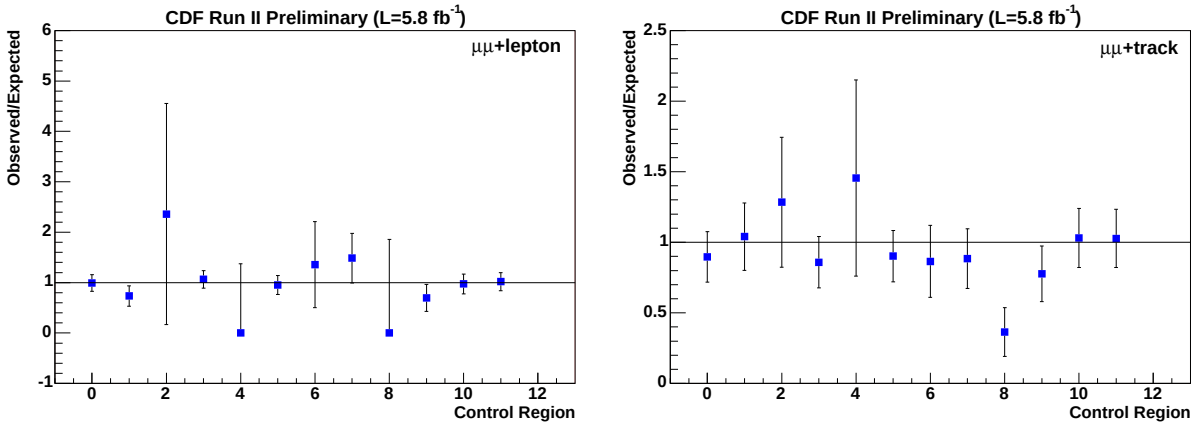

FIG. 14: $N_{\text{observed}}/N_{\text{expected}}$ ratio for $\mu\mu$+lepton (left) and $\mu\mu$+track (right) for all control and signal regions.

VI. SIGNAL-REGION RESULTS

Only when we achieve good understanding of the SM backgrounds in both event yields and kinematic distributions in our control regions, we turn our attention to the signal region, defined as $\not\!\!E_T > 15$ GeV, $N_{\text{jet}} \leq 1$ and ($M_{\ell\ell} < 76$ or $M_{\ell\ell} < 106$ GeV/c^2). Figures 15 and 16 show the observed dielectron and dimuon mass spectrum for ee+lepton and $\mu\mu$+lepton events in the signal region (along with the systematic uncertainties on the SM expectation). Also shown is our benchmark SUSY MC signal with mSUGRA parameters $m_0 = 60$ GeV/c^2, $\tan\beta = 3$, $A_0 = 0$, and $M_{1/2} = 190$ GeV/c^2. Figures 17 and 18 show the observed distribution of $\not\!\!E_T$ for ee+lepton and $\mu\mu$+lepton events in the signal region. Figures 19 and 20 show the observed dielectron and dimuon mass spectrum for ee+track and $\mu\mu$+track events in the signal region (along with the systematic uncertainties on the SM expectation). Figures 21 and 22 show the respective $\not\!\!E_T$ distributions. In the ee+lepton and $\mu\mu$+lepton low-dilepton-mass region we observe an excess of events that is not very significant. Our results overall are not inconsistent with the expectation from the SM background.

Tables IV-VII show the observed and expected trilepton yields. A secondary signal region with $\not\!\!E_T > 20$ GeV and no jet-multiplicity cut is also presented (Region 9).

A. Chargino-Neutralino Limit

Our trilepton signal results are interpreted in the mSUGRA model. To determine our acceptance, we use MC generated with the same way as background and normalized to the PROSPINO [18] NLO production cross section of chargino-neutralino, for both charges of

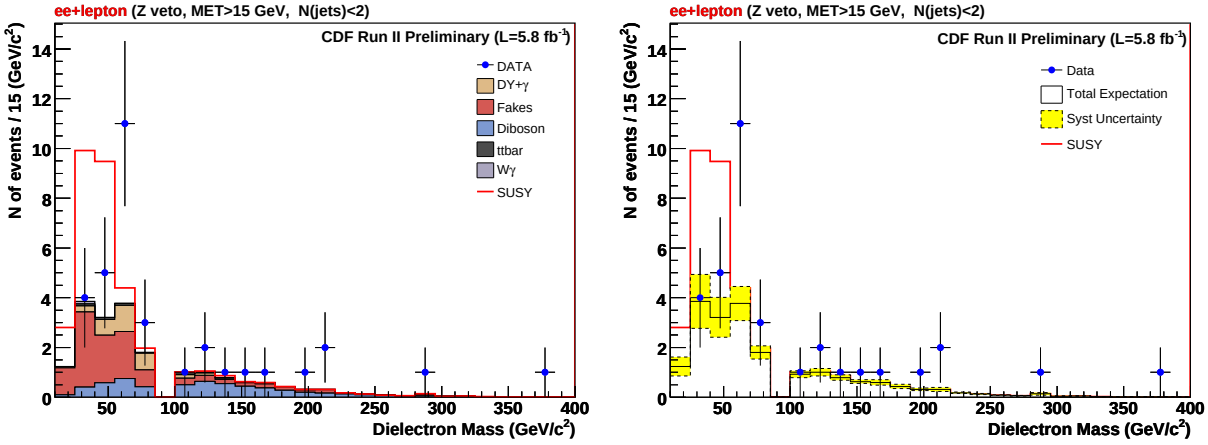

FIG. 15: Dielectron spectrum for ee+lepton events in the signal region ($\not\!\!E_T > 15$ GeV, $N_{\rm jet} \leq 1$ and exclusion of Z resonance). Right-hand plot shows the SM prediction systematic uncertainty.

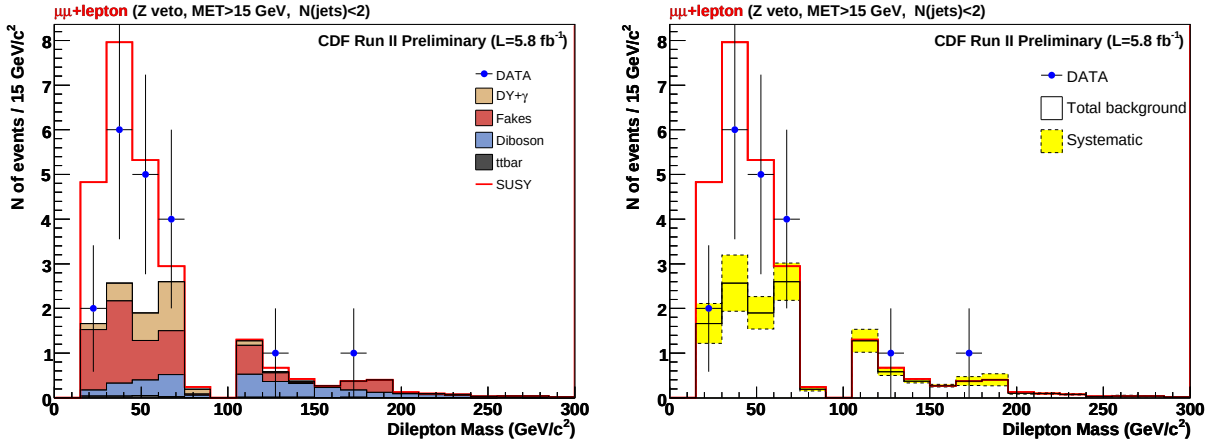

FIG. 16: Dimuon spectrum for $\mu\mu$+lepton events in the signal region ($\not\!\!E_T > 15$ GeV, $N_{\rm jet} \leq 1$ and exclusion of Z resonance). Right-hand plot shows the SM prediction systematic uncertainty.

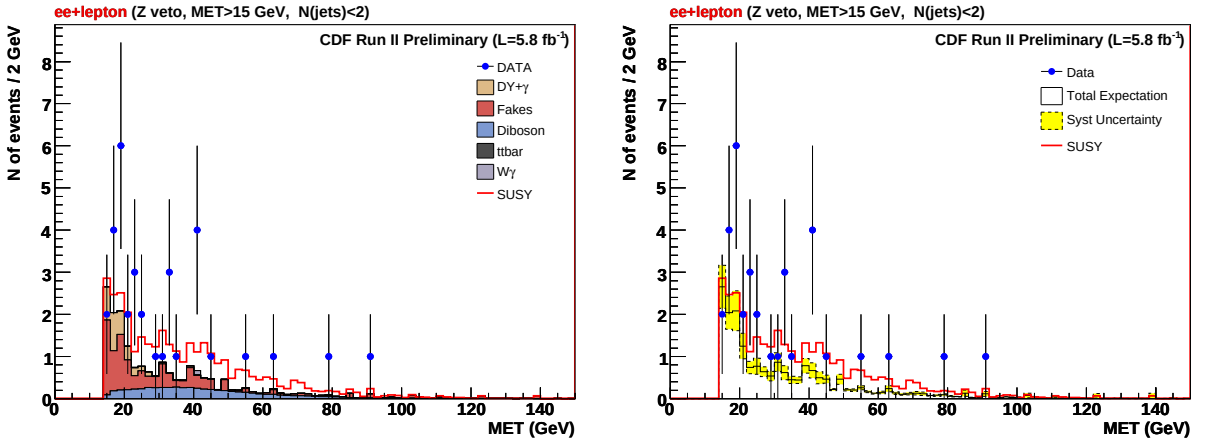

FIG. 17: Distribution of $\not\!\!E_T$ for ee+lepton events in the signal region ($\not\!\!E_T > 15$ GeV, $N_{\rm jet} \leq 1$ and exclusion of Z resonance). Right-hand plot shows the SM prediction systematic uncertainty.

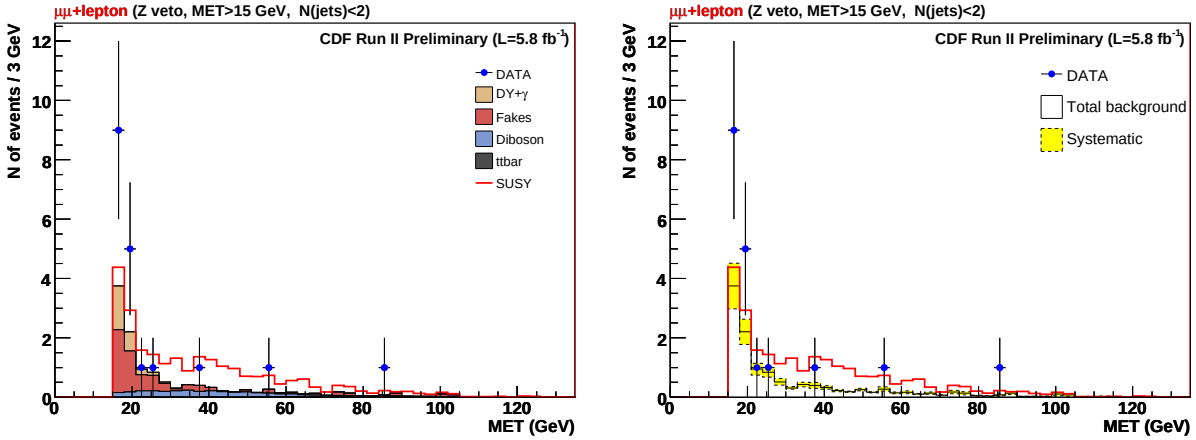

FIG. 18: Distribution of $\not\!\!E_T$ for $\mu\mu$+lepton events in the signal region ($\not\!\!E_T > 15$ GeV, $N_{\rm jet} \leq 1$ and exclusion of Z resonance). Right-hand plot shows the SM prediction systematic uncertainty.

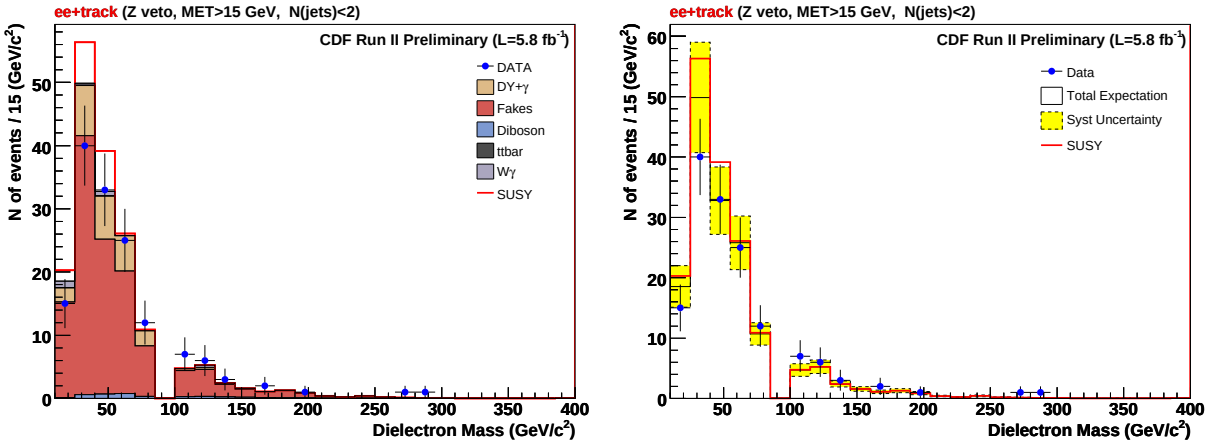

FIG. 19: Dielectron spectrum for ee+track events in the signal region ($\not\!\!E_T > 15$ GeV, $N_{\rm jet} \leq 1$ and exclusion of Z resonance). Right-hand plot shows the SM prediction systematic uncertainty.

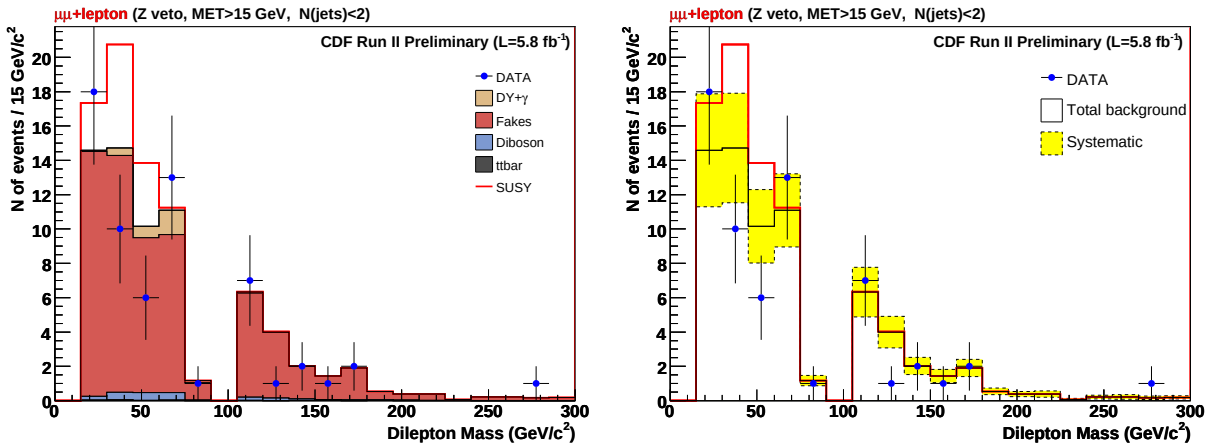

FIG. 20: Dimuon spectrum for $\mu\mu$+track events in the signal region ($\not\!\!E_T > 15$ GeV, $N_{\rm jet} \leq 1$ and exclusion of Z resonance). Right-hand plot shows the SM prediction systematic uncertainty.

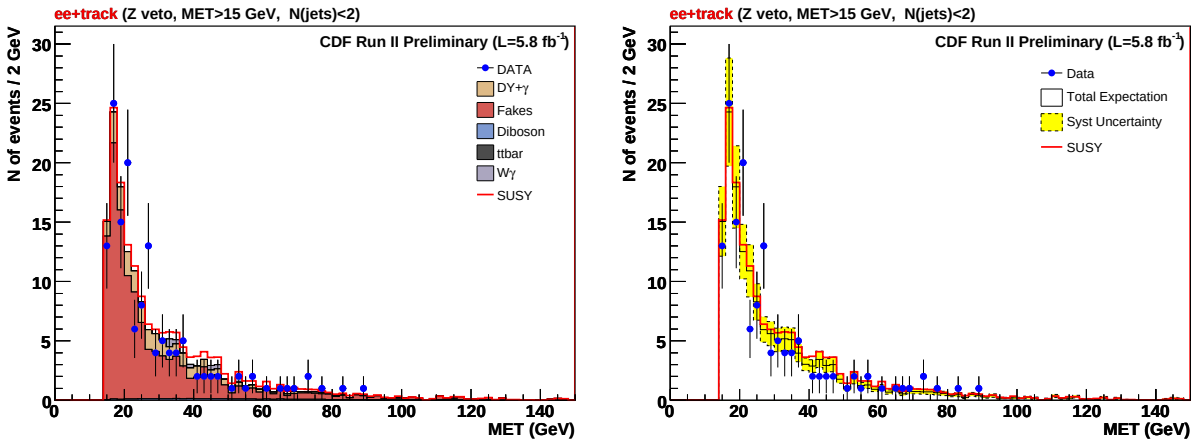

FIG. 21: Distribution of $\not\!\!E_T$ for ee+track events in the signal region ($\not\!\!E_T > 15$ GeV, $N_{\rm jet} \leq 1$ and exclusion of Z resonance). Right-hand plot shows the SM prediction systematic uncertainty.

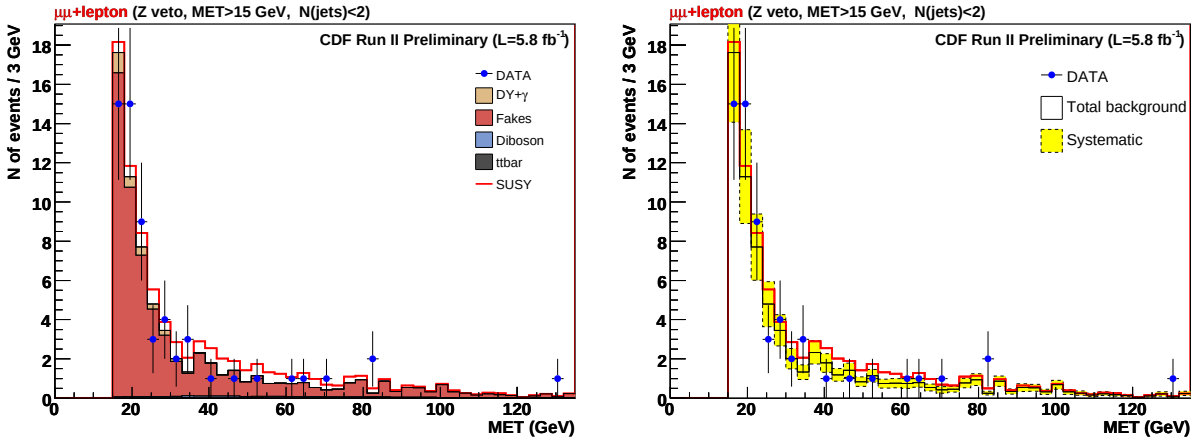

FIG. 22: Distribution of $\not\!\!E_T$ for $\mu\mu$+track events in the signal region ($\not\!\!E_T > 15$ GeV, $N_{\rm jet} \leq 1$ and exclusion of Z resonance). Right-hand plot shows the SM prediction systematic uncertainty.

chargino. The branching ratio (BR) to trileptons is determined by using the Les-Houches formatted SOFTSUSY/SDECAY) [19, 20] spectrum (and BR) generators. We repeated the procedure for all our signal MC samples, generated for the mSUGRA parameters $m_0 = 60$ GeV/c^2, $\tan\beta = 3$, $A_0 = 0$, and $M_{1/2} = 162 - 280$ GeV/c^2, which correspond to lightest chargino masses $M_{\tilde{\chi}_1^\pm} = 97 - 200$ GeV/c^2 and lightest neutralino masses $M_{\tilde{\chi}_1^0} = 55 - 108$ GeV/c^2.

We optimize our $M_{\ell\ell}$, $\not\!\!E_T$, and transverse-momenta selections individually for each of the above parameter-space values. For example, kinematically we expect a cut-off in the dilepton mass at about $M_{\ell\ell} = M_{\tilde{\chi}_1^\pm} - M_{\tilde{\chi}_1^0}$. Also, the expected signal $\not\!\!E_T$ increases as this difference increases (since it will give higher momentum to the missing LSP). The optimization figure of merit was the ratio of expected signal over expected background. In

addition, we apply tighter cuts on the lepton transverse momenta and on the subleading combinations of dilepton masses; the latter cuts reduce the diboson background. Table VIII shows the optimization cuts and table IX shows the expected background, expected chargino-neutralino signal, and observed events in the signal region, for our benchmark point ($m_0 = 60$ GeV/c^2, $\tan\beta = 3$, $A_0 = 0$, and $M_{1/2} = 190$ GeV/c^2) for ee+lepton, ee+track, $\mu\mu$+lepton, and $\mu\mu$+track.

Optimization cuts	
$M_{\ell_1\ell_2}$	$> M_{\tilde{\chi}_1^\pm} - M_{\tilde{\chi}_1^0}$
$M_{\ell_1\ell_3}$	< 75 GeV/c^2
$M_{\ell_2\ell_3}$	< 75 GeV/c^2
$\not\!\!E_T$	> 25 GeV
$p_{T,2}$	$(> 8$ and $< 36 - 65)$ GeV/c
$p_{T,3}$	> 8 GeV/c

TABLE VIII: The optimization cuts on the three dilepton-mass combinations, $\not\!\!E_T$, and lepton transverse momenta. The leading dilepton mass cut and second-leading momentum transverse momentum cut are mSUGRA-point dependent.

Optimized Trilepton Yields for Benchmark			
Channel	**SM background**	**SUSY signal**	**Observation**
ee+lepton	1.5 ± 0.4	7.6 ± 0.9	**3**
ee+track	11.7 ± 1.7	8.0 ± 0.9	**13**
$\mu\mu$+lepton	0.5 ± 0.1	6.7 ± 0.8	**0**
$\mu\mu$+track	3.9 ± 1.0	6.5 ± 0.8	**3**

TABLE IX: The optimized trilepton yields in the signal region. The chargino-neutralino signal corresponds to the mSUGRA parameters $m_0 = 60$ GeV/c^2, $\tan\beta = 3$, $A_0 = 0$, and $M_{1/2} = 190$ GeV/c^2

The limit is determined using a modified frequentist approach (CL_s method) [21, 22] and by treating all the channels independently. Figure 23 shows our upper cross-section 95% CL limit as a function of the chargino mass. Intersection with the NLO theoretical curve gives us the lower chargino mass limit. At 95% CL, we exclude $\sigma(\tilde{\chi}_1^\pm\tilde{\chi}_2^0) \times \mathrm{BR}(\ell\ell\ell)$ above 0.1 fb and chargino masses below 168 GeV/c^2. We also exclude a region in the $m_{1/2}$ vs. m_0 mSUGRA parameter space at 95% CL, shown in Figure 24 in comparison with the LEP slepton exclusion [23–27] and the CMS 35 pb^{-1} exclusion [28]. Figures 25 and 26 show the exclusion limit in the $m_{\tilde{\chi}_1^0}$ vs. $m_{\tilde{\tau}}$ and $m_{\tilde{\chi}_2^0}$ vs. $m_{\tilde{\tau}}$ space respectively. All limits were the best in the world at the time of release (late August 2011).

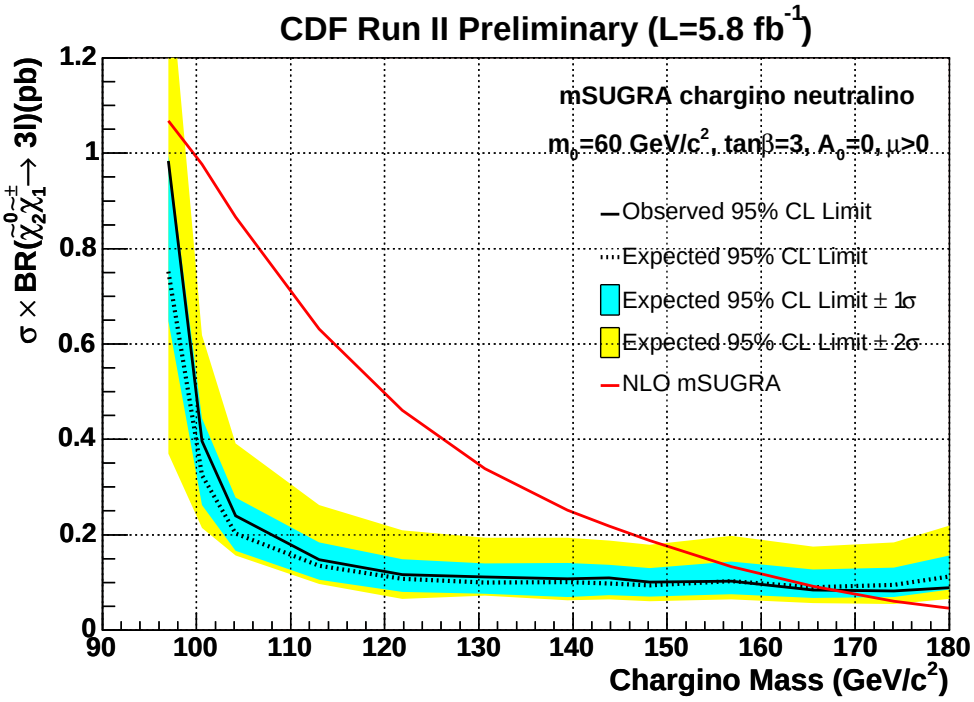

FIG. 23: The 95% CL upper limit on the chargino-neutralino production cross section with subsequent trileptonic decay as a function of the chargino mass. The intersection with the NLO SUSY prediction gives as the 95% CL lower limit on the chargino mass at 168 GeV/c^2.

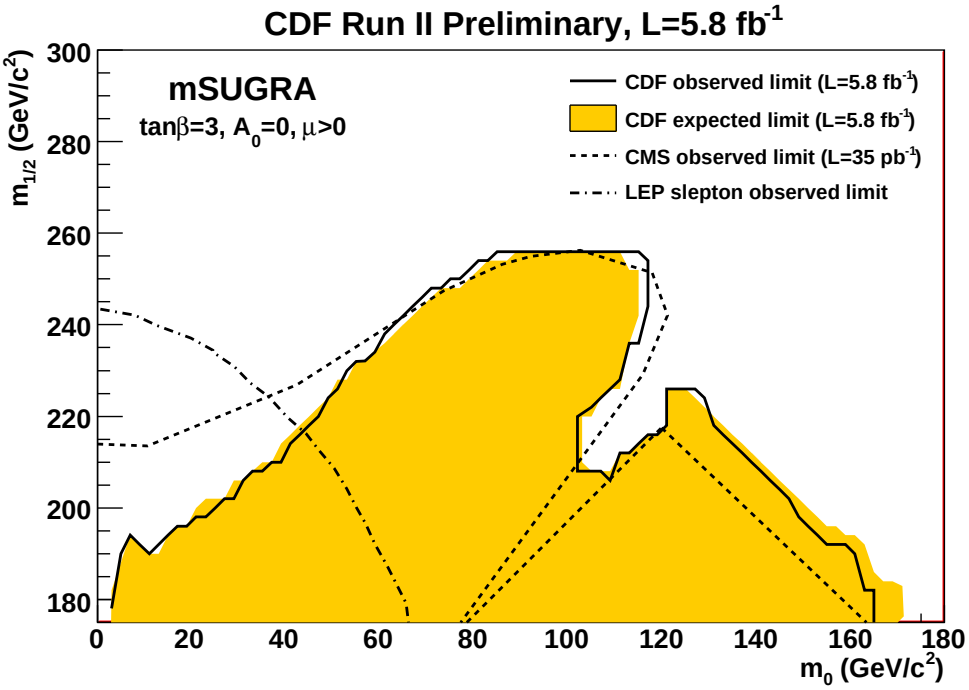

FIG. 24: The CDF $m_{1/2}$ vs. m_0 95% CL exclusion compared with the CMS 35 pb^{-1} exclusion [28] and with the LEP slepton exclusion [23–27].

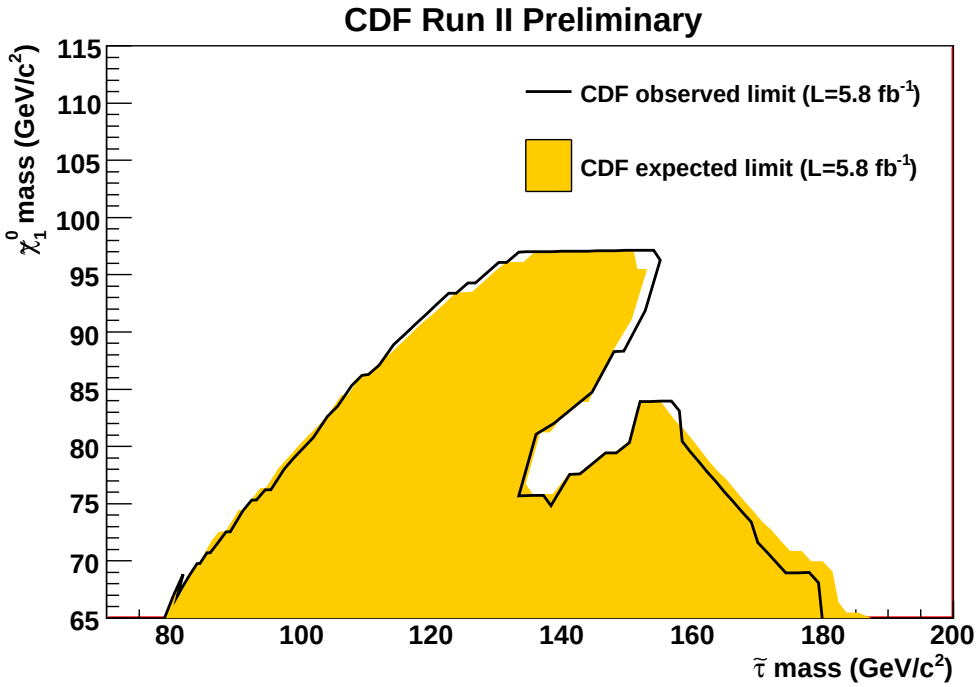

FIG. 25: CDF expected and observed 95% CL exclusion in the $m_{\tilde{\chi}_1^0}$ vs. $m_{\tilde{\tau}}$ space.

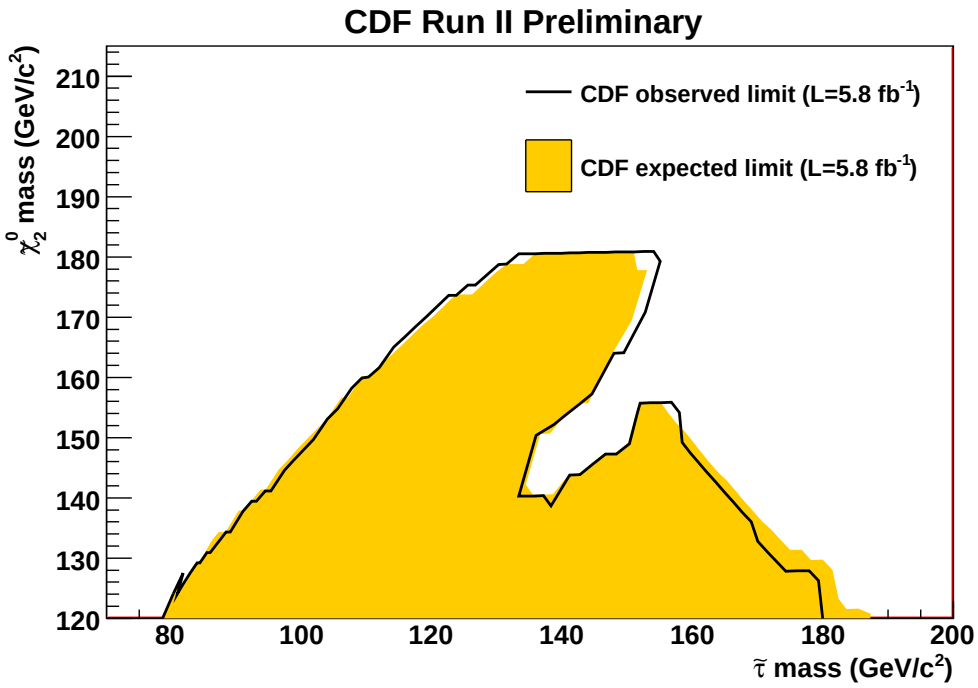

FIG. 26: CDF expected and observed 95% CL exclusion in the $m_{\tilde{\chi}_2^0}$ vs. $m_{\tilde{\tau}}$ space.

VII. CONCLUSIONS

We presented the trilepton+$\not\!\!E_T$ search for new physics, the golden Tevatron channel for SUSY searches. Although inspired by SUSY, we did not optimize our selection specifically for this theory. In this analysis we expand our leptonic acceptance geometrically (forward parts of the detector), kinematically (as low p_T as possible) and with the inclusion of tau leptons decaying hadronically. After good understanding of the SM backgrounds in 24 dilepton and 40 trilepton control regions, we observe signal-region results with a slight excess not incompatible with expectation. We interpret the results in the mSUGRA channel, and we set a limit in the chargino-neutralino production cross-section with subsequent decay to trileptons. At 95% CL, we exclude $\sigma(\tilde{\chi}_1^{\pm}\tilde{\chi}_2^0) \times \mathrm{BR}(\ell\ell\ell)$ above 0.1 fb and chargino masses below 168 GeV/c^2. We also set a limit in the $m_{1/2}$ vs. m_0 mSUGRA parameter space, as well as in the $m_{\tilde{\chi}_{1,2}^0}$ vs. $m_{\tilde{\tau}}$ space. Our limits are the best in the world at the time of release, but they are expected to be improved soon by LHC.

VIII. ACKNOWLEDGMENTS

We thank the Fermilab staff and the technical staffs of the participating institutions for their vital contributions. This work was supported by the U.S. Department of Energy and National Science Foundation; the Italian Istituto Nazionale di Fisica Nucleare; the Ministry of Education, Culture, Sports, Science and Technology of Japan; the Natural Sciences and Engineering Research Council of Canada; the National Science Council of the Republic of China; the Swiss National Science Foundation; the A.P. Sloan Foundation; the Bundesministerium für Bildung und Forschung, Germany; the Korean World Class University Program, the National Research Foundation of Korea; the Science and Technology Facilities Council and the Royal Society, UK; the Institut National de Physique Nucleaire et Physique des Particules/CNRS; the Russian Foundation for Basic Research; the Ministerio de Ciencia e Innovación, and Programa Consolider-Ingenio 2010, Spain; the Slovak R&D Agency; the Academy of Finland; and the Australian Research Council (ARC).

[1] H. Baer *et al.*, Phys. Rev. D **61**, 095007 (2000).

[2] T. Aaltonen *et al.* (CDF Collaboration), Phys. Rev. Lett. **102**, 121801 (2009).

[3] T. Aaltonen *et al.* (CDF Collaboration), Phys. Rev. Lett. **99**, 191806 (2007).

[4] T. Aaltonen *et al.* (CDF Collaboration), Phys. Rev. D **77**, 052002 (2008).

[5] T. Aaltonen *et al.* (CDF Collaboration), Phys. Rev. D **79**, 052004 (2009).

[6] T. Aaltonen *et al.* (CDF Collaboration), Phys. Rev. Lett. **101**, 251801 (2008).

[7] T. Aaltonen *et al.* (CDF Collaboration), CDF public note 9817 (2009).

[8] V. M. Abazov *et al.* (DØ Collaboration), Phys. Lett. B **680**, 34 (2009).

[9] D. Acosta *et al.* (CDF Collaboration), Phys. Rev. D **71**, 032001 (2005).

[10] R. Downing *et al.*, Nucl. Instrum. Methods A **570**, 36 (2007).

[11] F. Abe *et al.* (CDF Collaboration), Phys. Rev. D **45**, 1448 (1992).

[12] T. Sjöstrand, L. Lönnblad, and S. Mrenna, PYTHIA 6.2, arXiv:hep-ph/0108264.

[13] H. Lai *et al.* (CTEQ Collaboration), Eur. Phys. J. C **12**, 375 (2000).

[14] R. Brun, R. Hagelberg, M. Hansroul, and J. Lasalle, CERN report CERN-DD-78-2-REV, (1978).

[15] A. D. Martin, W. J. Stirling, R. S. Thorne, G. Watt, Eur. Phys. J. **C63**, 189 (2009); J. M. Campbell and R. K. Ellis, Phys. Rev. D **60**, 113006 (1999); N. Kidonakis and R. Vogt, Phys. Rev. D **78**, 074005 (2008).

[16] M. Vogel, Ph.D. thesis, University of New Mexico, expected 2011.

[17] T. Aaltonen *et al.* (CDF Collaboration), Phys. Rev. D **79**, 052004 (2009).

[18] W. Beenakker *et al.*, Phys. Rev. Lett. **83**, 3780 (1999).

[19] B. C. Allanach, Comput. Phys. Commun. **143**, 305 (2002), arXiv:hep-ph/0104145.

[20] M. Muhlleitner, A. Djouadi, Y. Mambrini, Comput. Phys. Commun. **168**, 46 (2005), arXiv:hep-ph/0311167.

[21] T. Junk, Nucl. Instrum. Methods A **434**, 435 (1999).

[22] A. Read, J. Phys. G **28**, 2693 (2002).

[23] ALEPH Collaboration, Phys. Lett. B **526**, 206 (2002).

[24] ALEPH Collaboration, Phys. Lett. B **583**, 247 (2004).

[25] DELPHI Collaboration, Eur. Phys. J. C **31**, 421 (2003).

[26] L3 Collaboration, Phys. Lett. B **580**, 37 (2004).

[27] OPAL Collaboration, Eur. Phys. J. C **32**, 453 (2004).

[28] CMS collaboration, Phys. Lett. B **704**, 411 (2011).